Pre-synaptic HCN1 channels regulate excitatory neurotransmission at select cortical synapses by altering Ca$_V$3.2 Ca^{2+} channel activity

Zhuo Huang[1], **Rafael Lujan**[2], **Ivan Kadurin**[3], **Victor N. Uebele**[4], **John J. Renger**[4], **Annette C. Dolphin**[3], and **Mala M. Shah**[1,*]

[1]Dpt. Pharmacology, The School of Pharmacy, University of London, London, WC1N 1AX, UK

[2]Dpt. Ciencias Medicas, Centro de Investigación en Discapacidades Neurológicas (IDINE), Universidad de Castilla-La Mancha, Albacete, Spain

[3]Dpt. Neuroscience, Physiology and Pharmacology, University College, London, WC1E 6BT, UK

[4]Dpt. Depression and Circadian Rhythms, Merck Research Laboratories, West Point, PA 19486, USA

Abstract

The Hyperpolarization-activated Cyclic Nucleotide-gated (HCN) channels are subthreshold, voltage-gated ion channels that are highly expressed in hippocampal and cortical pyramidal cell dendrites, where they play an important role in regulating synaptic potential integration and plasticity. Here, we demonstrate that HCN1 subunits are also localized to the active zone of mature asymmetric synaptic terminals targeting mouse entorhinal cortical layer III pyramidal neurons. We found that HCN channels inhibit glutamate synaptic release by suppressing the activity of low threshold voltage-gated T- (Ca$_V$3.2) type Ca^{2+} channels. In agreement, electron microscopy showed the co-localisation of pre-synaptic HCN1 and Ca$_V$3.2 subunit. This represents a novel mechanism by which HCN channels regulate synaptic strength and thereby neural information processing and network excitability.

Hyperpolarization-activated Cyclic Nucleotide-gated (HCN) channels are low threshold, voltage-gated ion channels with very unusual biophysical properties[1]. These channels are open at potentials more negative to −50 mV and are important for regulating neuronal resting membrane potential (RMP). In addition, the channels are permeable to Na$^+$ and K$^+$ and form an inward current at rest, thereby depolarizing RMP. Interestingly, in the hippocampus and cortex, they are highly localized to pyramidal cell dendrites[2, 3]. Here, by regulating the RMP and in this way the biophysical properties of other ion channels as well as by modulating the membrane resistance, they influence excitatory post-synaptic potential (EPSP) kinetics and integration[4-7]. These effects are likely to contribute substantially to synaptic plasticity and thus, processes such as information storage[8-12]. Indeed a reduction in HCN channel expression has been associated with enhanced learning[8, 9].

Emerging evidence, though, suggests that in addition to their dendritic localization, HCN1 channels may be present on certain axons and synaptic terminals in the hippocampus, cortex

and other regions of the brain[3], [13]-[15]. Indeed, pre-synaptic HCN channel current, I_h, has been indicated to affect inhibitory synaptic transmission in the rodent cerebellum, hippocampus and basal ganglia[14], [16], [17], though the mechanism by which this occurs is unknown. However, in contrast to invertebrate neurons where I_h has been shown to influence excitatory synaptic release[18], [19], an explicit role for I_h in regulating excitatory basal synaptic transmission in mammals has not yet been revealed. This is despite HCN subunit expression being detected in some immature mammalian glutamatergic pathways[13] and functional I_h recorded from pre-synaptic immature terminals in the calyx of Held[20]. In this study, we demonstrate that HCN1 channels are present at the active zone of mature glutamatergic cortical synaptic terminals establishing contact with entorhinal cortical (EC) layer III cells where they decrease neurotransmission by restricting Ca^{2+} entry via pre-synaptic T ($Ca_V3.2$) -type Ca^{2+} channels. Since changes in synaptic strength are pivotal to induction and maintenance of synaptic plasticity[21] and given that EC layer III neurons are likely to be involved in memory formation and spatial navigation[22], [23], our results indicate that this is a novel mechanism by which HCN1 subunits may contribute to such physiological processes.

Results

HCN1 channels modulate glutamatergic synaptic release onto EC layer III cells exclusively

Synaptic release plays a central role in regulating individual neuronal as well as neural network excitability. Thus, elucidating the factors regulating synaptic transmission is critical for understanding how neural circuits function. In an earlier study[4], we had observed that a loss of I_h enhances synaptic transmission onto mature EC layer III pyramidal neurons, the principal cell type within layer III[24]. This is likely to have been, at least partly, due to enhanced feed forward excitation resulting from pyramidal cell hyperexcitability. However, since HCN subunits may be present at certain synaptic terminals[13]-[17], [20], it is possible that this effect could be due to changes in synaptic release *per se* by altered pre-synaptic HCN channel function.

To test this, we initially recorded non-evoked miniature excitatory post-synaptic currents (mEPSC) in the presence of tetrodotoxin (TTX, 1 μM) and GABA receptor inhibitors at a fixed potential of −70 mV from mouse EC layer III neurons (Fig 1a) using the whole-cell voltage clamp technique (as described previously[14], [16], [17], see **Methods**). To exclude the effects of post-synaptic HCN channels[12] and to reduce errors due to space-clamp[25], 15 μM ZD7288 was incorporated in the patch pipette in all our experiments, unless otherwise stated. Intracellular ZD7288 enhanced the outward holding current, indicating that the post-synaptic neuronal resting membrane potential (RMP) was hyperpolarized (Supplementary Table 1). The mEPSC rise and decay times were also slowed down as would be expected from blocking post-synaptic HCN channels (see Refs.[4], [5], [24]). Including ZD7288 in the patch pipette, though, had no effect on mEPSC frequency indicating this did not affect synaptic release *per se* (Supplementary Table 1). Further, substituting $KMeSO_4$ with $CsMeSO_4$ in the intracellular solution did not alter either somatic or dendritic mEPSC frequency, amplitude and kinetics (Supplementary Table 1), indicating that the errors due to space-clamp were not reduced further by blocking post-synaptic K^+ channels[25].

To determine if functional HCN channels are present pre-synaptically, we bath-applied ZD7288 (15 μM) for 15 min only to exclude any potential non-specific effects of the compound on synaptic transmission[26]. This concentration was deemed specific as it enhances wildtype dendritic excitability whilst having little effect on *HCN1−/−* dendrites (see Ref. [4]). Intriguingly, external application of ZD7288 enhanced wildtype somatic mEPSC frequency by 113.8 ± 19.1% (n=7, p < 0.01; Fig 1b). The outward holding current as well as mEPSC amplitude, rise-times and decay time constants were not further affected

(Fig 1b). Further, 15 min external application of another I_h blocker, zatebradine[27], [28] (10 μM) also enhanced mEPSC frequency in a comparable manner without affecting amplitude or kinetics (Supplementary Fig 1a). In the above experiments, ZD7288 was included in the internal patch pipette solution. However, even when this was not present in the internal solution, external application of ZD7288 still amplified wildtype mEPSC frequency by $108.3 \pm 14.8\%$ (n=6). In these experiments, the decay time constant increased significantly from 7.9 ± 0.6 (n=6) to 10.0 ± 0.5 (n=6, p < 0.05), as would be predicted by blocking post-synaptic HCN channels.

Since dendrites receive the majority of excitatory synaptic inputs[29], we also recorded mEPSCs from EC layer III apical dendrites at a distance of 120 -150 μm from the soma (Fig 1c). The frequency, but not amplitude or kinetics, of dendritic mEPSCs was increased by application of ZD7288 by $69.7 \pm 5.3\%$ (n=5; Fig 1c). This effect was not significantly different (p=0.1) to that observed at the soma. The above results indicate that synapses targeting EC layer III neurons contain pre-synaptic I_h.

HCN1 subunits are likely to be predominantly expressed in the EC[3], [4]. We, therefore, compared *HCN1−/−* and wildtype mEPSCs recorded from layer III neurons. Since ZD7288 was present in the internal pipette solution, wildtype and *HCN1−/−* outward holding current and mEPSC kinetics were similar (Supplementary Table 1). Interestingly, the average somatic, but not dendritic, *HCN1−/−* mEPSC amplitudes were smaller than in wildtypes (Supplementary Table 1). Importantly, though, *HCN1−/−* mEPSC frequency was significantly greater than in wildtypes (Fig 1b, c, Supplementary Table 1). Moreover, omitting ZD7288 from the internal pipette solution did not affect *HCN1−/−* mEPSC frequency or kinetics (Supplementary Table 1). Additionally, 15 min bath application of ZD7288 or zatebradine had no effect on somatic or dendritic *HCN1−/−* mEPSC frequency, amplitude or shape (Fig 1b, c; Supplementary Fig 1b). These findings confirm that the enhanced wildtype mEPSC frequency caused by pharmacological blockers of I_h is likely to be due to HCN channel block and not non-specific effects of the compounds[26]. These results also indicate that pre-synaptic HCN1 channels are likely to be involved in regulating excitatory spontaneous release from synapses localised to EC layer III neurons.

We then recorded miniature inhibitory synaptic currents (mIPSCs) to determine if HCN channels were also present pre-synaptically on interneurons. In contrast to mEPSCs, somatic EC layer III mIPSCs were unaffected by 15 min bath-application of ZD7288 (Supplementary Fig 2a). Moreover, mIPSC frequency, amplitude and kinetics recorded from wildtype and *HCN1−/−* neurons did not differ (Supplementary Fig 2b). These findings suggest that in the EC, HCN1 channels selectively regulate glutamatergic synaptic release.

We next asked whether HCN1 channels were present at excitatory synapses targeting other principal EC neurons, particularly layer II stellate (Fig 2a) and layer V pyramids (Fig 2c). Intriguingly, application of ZD7288 had no effect on wildtype mEPSC frequency, amplitudes or kinetics recorded from the soma of these neurons (Fig 2b, d). In addition, there were no differences between *HCN1−/−* and wildtype layer II and layer V mEPSCs (Fig 2). Since layer III pyramid dendrites are present in layer II and mEPSC frequency onto these is altered by pharmacological block of I_h or HCN1 deletion (Fig 1c), these results suggest that HCN1 channels are predominantly located at glutamatergic synaptic terminals contacting EC layer III pyramids.

HCN1 subunits are present at the active zone of selective terminals

To determine if HCN1 subunits are located on EC synaptic terminals, we carried out electron microscopy studies using a pre-embedding immunogold method (see **Methods**). We counted 2752 particles in the medial EC from sections obtained from 3 wildtype mice.

72.2 ± 0.8% of HCN1 immunogold particles were observed along the extra-synaptic plasma membrane of dendritic shafts and spines (Fig 3a, e), confirming that HCN channels are largely present in EC dendrites. Interestingly, 27.8 ± 1.0% of immunogold particles were located at pre-synaptic sites (Fig 3b, e).

We further analysed the distribution of pre-synaptic particles. Of 153 immunogold particles that were detected on synaptic terminals, the majority ((129/153, 84%) of HCN1 immunogold particles were localized at terminals establishing asymmetrical excitatory synapses with pyramid dendritic spines (Fig 3b). Of these, 71% (92/129) were present in the active zone and 29% (37/129) in pre-synaptic terminal membranes. In contrast, only 16% (24/153 particles in 8 synapses) were located in the axonal plasma membranes establishing symmetrical synapses (Fig 3c). Interestingly, very few immunogold particles were observed in layer V (data not shown). No staining occurred if either the primary or secondary antibodies were omitted. Further, no signal was detected in *HCN1−/−* sections obtained from 4 mice under either light (Supplementary Fig 3) or electron microscopy (Fig 3d). Thus, these results together with the electrophysiological results suggest that HCN1 subunits are present at excitatory pre-synaptic terminals synapsing onto EC layer III neurons. These data are also consistent with our findings that ZD7288 only alters spontaneous excitatory synaptic transmission, and not inhibitory synaptic transmission, at layer III neurons (Fig 1, Supplementary Fig 1 and Supplementary Fig 2).

Enhanced Ca^{2+} dependence of *HCN1−/−* mEPSCs

How do pre-synaptic HCN1 subunits regulate synaptic transmission at synapses targeting EC layer III neurons? Since acute treatment of ZD7288 in wildtype neurons results in enhanced mEPSC frequency, it suggests that pre-synaptic HCN1 subunits do not affect synaptogenesis. Nevertheless, we compared the number of synapses in superficial EC layers (layers I-III) between wildtypes and *HCN1−/−* mice using electron microscopy. From sections obtained from 3 wildtype and 4 *HCN1−/−* mice, no obvious differences in the number of synapses were detected (Supplementary Fig 4), indicating that HCN1 subunits on synaptic terminals are likely to reduce synaptic transmission by directly affecting release probability.

One possible mechanism by which pre-synaptic HCN1 channels may regulate synaptic transmission is by limiting Ca^{2+} influx, as has been suggested to occur in dendrites[7]. Recent studies suggest that spontaneous as well as action potential-driven synaptic release may be dependent upon Ca^{2+} entry via voltage-gated Ca^{2+} channels (VGCC)[30-34]. We, therefore, tested if the mEPSCs recorded from layer III soma were Ca^{2+}-dependent. Replacement of Ca^{2+} in the extracellular solution with an equal concentration of Mg^{2+} reversibly reduced wildtype mEPSC frequency by 56.3 ± 5.1% (n=9, p < 0.01) within 5 min (Fig 4a, b). Interestingly, substitution of Ca^{2+} with Mg^{2+} lowered *HCN1−/−* mEPSC frequency by 70.1 ± 3.6% (n=9, p < 0.01, Fig 4a) in a reversible manner (Fig 4a, b). This decrease in *HCN1−/−* mEPSC frequency was significantly (p = 0.04) greater than that in wildtypes. Neither the amplitudes nor the time constants of wildtype or *HCN1−/−* mEPSCs were affected by replacing external Ca^{2+} with Mg^{2+}. The outward holding current, though, was reduced significantly to a similar extent in wildtype and *HCN1−/−* neurones (average holding current in the presence of Ca^{2+} in wildtypes and *HCN1−/−* cells = 30.0 ± 7.9 pA (n=9) and 39.4 ± 20.0 pA (n=9) respectively; holding current without Ca^{2+} in wildtypes and *HCN1−/−* pyramids = 5.0 ± 7.1 pA (n=9, p < 0.05) and 10.0 ± 20.3 (n=9, p < 0.05)). Given the larger Ca^{2+} dependence of *HCN1−/−* mEPSCs, these results imply that pre-synaptic HCN1 channels regulate synaptic release by constraining Ca^{2+} influx into terminals. Indeed, in the absence of extracellular Ca^{2+}, bath application of ZD7288 no longer increased mEPSC frequency in wildtypes (Fig 4c).

HCN1 channels inhibit mEPSC frequency by limiting T-type Ca^{2+} channel activity

We next asked if Ca^{2+} entry through specific VGCCs contributes to generation of spontaneous mEPSCs and whether pre-synaptic HCN1 channels limit the activity of particular VGCCs. To investigate this, we first examined the effects of various pharmacological inhibitors of VGCCs on wildtype mEPSC frequency. The P/Q Ca^{2+} channel blocker, ω -agatoxin IVA[35, 36] (100 nM) and the N-type Ca^{2+} channel inhibitor, ω-conotoxin GVIA[35, 36] (100 nM) reduced wildtype mEPSC frequency by 47.3 ± 3.1% (n=11, Supplementary Fig 5) and 22.2 ± 4.7% (n=9, Supplementary Fig 5) respectively, without affecting amplitude or kinetics (Supplementary Table 2). The effects occurred within 10 min of bath application. ω -agatoxin IVA and ω-conotoxin GVIA co-application decreased mEPSC frequency by 48.6 ± 5.5% (n=6, Supplementary Fig 5). In contrast, neither the L-type Ca^{2+} channel inhibitor, nifedipine[35, 36] (2 μM), the R-type Ca^{2+} channel antagonist, SNX-482[37] (200 nM) nor the selective T-type Ca^{2+} channel blockers, mibefradil[36] (10 μM), TTA-P2 (1 μM)[38], TTA-A2[39, 40] (500 nM) had any effect on wildtype mEPSCs (Supplementary Fig 5, Supplementary Table 2). Since wildtype mEPSC frequency inhibition in the presence of ω -agatoxin IVA and ω-conotoxin GVIA together is comparable to that resulting from removal of extracellular Ca^{2+} (Fig 4a, b), it suggests that in these neurones, Ca^{2+}- influx via P/Q- and N-type generates Ca^{2+}-dependent mEPSCs.

Next we tested whether the ZD7288 induced enhancement in wildtype mEPSC frequency (Fig 1) could be occluded by pre-treatment with either ω -agatoxin IVA (100 nM) or ω-conotoxin GVIA (100 nM). Co-application of ZD7288 with either ω-agatoxin IVA or ω-conotoxin GVIA or both increased mEPSC frequency in a comparable manner to that produced by ZD7288 alone (Fig 5c). Moreover, in the presence of either nifedipine or SNX-482, ZD7288 also augmented mEPSC frequency (Fig 5c). However, intriguingly, the effects of ZD7288 on mEPSC frequency were prevented by pre-treatment with three different inhibitors of the low voltage-activated T-type Ca^{2+} channels: mibefradil (10 μM) as well as the more potent and selective inhibitors TTA-P2[38-40] (1μM) and TTA-A2[39, 40] (500 nM) (Fig 5a, c). The latter two have been shown to have no effects on other VGCC in either heterologous expression systems[39, 40] or neurons[38]. These findings suggest that inhibition of HCN1 channels enhances excitatory synaptic transmission by altering T-type Ca^{2+} channel activity.

To investigate this further, we explored the effects of T-type Ca^{2+} channel blockers on *HCN1−/−* mEPSC frequency. In contrast to the results obtained in wildtypes (Supplementary Fig 5), mibefradil (10 μM), TTA-A2 (500 nM) and TTA-P2 (1 μM) significantly reduced *HCN1−/−* somatic mEPSC frequency by 35.7 ± 4.8% (n=6, p < 0.05), 49.0 ± 4.8% (n=7, p < 0.05) and 50.4 ± 4.4% (n=6. P < 0.05) respectively (Fig 5b, d), whilst having no effect on amplitudes or time constants (Supplementary Table 3). As mibefradil may inhibit R-type Ca^{2+} channels too[41], we tested the effects of SNX-482 (200 nM) on *HCN1−/−* mEPSCs. 15 min application of SNX-482 had no effect on these (Fig 5d). To verify that T-type Ca^{2+} channels expression is not modified in *HCN1−/−* mice, we did Western blot analysis using Ca$_V$3.1 and Ca$_V$3.2 antibodies. We were unable to detect any Ca$_V$3.1 protein expression in wildtype or *HCN1−/−* EC. However, bands corresponding to the size of Ca$_V$3.2 proteins expressed in tsA-201 cells were present in wildtype and *HCN1−/−* EC samples (Supplementary Fig 6a, 7a). Semi-quantitative analysis indicated that there was no difference in expression of this between wildtype and *HCN1−/−* tissue (Supplementary Fig 6a, 7a). These findings re-affirm that a decrease in pre-synaptic HCN channel function leads to increased contribution of T-type Ca^{2+} channel activity in modulating basal glutamatergic synaptic release.

Co-localisation of HCN1 and Ca$_V$3.2 subunits on EC synaptic terminals

Since T-type Ca^{2+} channel inhibitors prevent the effects of ZD7288, it raises the possibility that these and HCN1 channels co-exist on the same pre-synaptic terminals. To investigate this, we took advantage of Ca$_V$3.1 and Ca$_V$3.2 antibodies to examine the localization of Ca$_V$3 and HCN1 subunits in wildtype EC. For these particular experiments, the anti-HCN1 antibody was visualized using an immunoperoxidase reaction and the anti-Ca$_V$3 antibody by a silver-intensified immunogold reaction (see **Methods**). Consistent with the Western blot data, Ca$_V$3.1 labelling could not be detected. However, remarkably, Ca$_V$3.2 immunogold particles were present on asymmetrical synaptic terminals (Fig 6a) in sections obtained from 3 wildtype mice. Approximately 84% of these were present on axons pre-labelled with HCN1. HCN1 and Ca$_V$3.2 co-labelling was noticeable on spines and dendrites too (Supplementary Fig 8). No Ca$_V$3.2 signal was identified on sections obtained from 3 *Ca$_V$3.2–/–* mice under either electron (Fig 6a) or light microscopy (Supplementary Fig 9). Moreover, no specific labelling was observed if the primary antibody was omitted or replaced with normal serum. In addition, the selective location of signals in structures labelled with only one or the other of the signalling products within the same section, as well as having side by side double-labelled structures, showed that our procedures did not produce false-positive double-labelling results. These results, thus, indicate that Ca$_V$3.2 and HCN1 subunits co-localise on synaptic terminals.

mEPSCs onto *Ca$_V$3.2$^{-/-}$* neurons were unaffected by HCN channel inhibition

Since T-type Ca^{2+} channels and HCN channels can co-exist on synaptic terminals (Fig 6a) and T-type Ca^{2+} channel blockers prevented the increase in mEPSC frequency by the HCN channel inhibitor, ZD7288 (Fig 5a, c), we hypothesized that HCN channel blockers may not affect excitatory synaptic transmission in *Ca$_V$3.2–/–* tissue. We, therefore, recorded mEPSCs from EC layer III neurons present in slices obtained from wildtype and *Ca$_V$3.2–/–* mice[42]. As in previous experiments, ZD7288 (15 µM) was included in the patch pipette to inhibit post-synaptic HCN channels. Wildtype and *Ca$_V$3.2–/–* mEPSC frequency, amplitude and kinetics were very similar (Supplementary Table 4), confirming that Ca$_V$3.2 channels do not modulate basal excitatory synaptic transmission. Interestingly, 15 min application of ZD7288 (15 µM) had little effect on *Ca$_V$3.2–/–* mEPSCs (Fig 6b) but enhanced wildtype mEPSC frequency (Fig 6b). HCN1 protein levels were similar Ca$_V$3.2 wildtype and null EC (Supplementary Fig 6b, 7b), indicating that the lack of effect of ZD7288 on *Ca$_V$3.2–/–* mice is not likely to be due to altered HCN1 expression. These results further support the notion that block of pre-synaptic HCN channels increases excitatory synaptic transmission by enhancing Ca^{2+} entry via pre-synaptic Ca$_V$3.2 Ca^{2+} channels.

Hyperpolarization enhances pre-synaptic T-type Ca^{2+} channel activation

Next, we wondered how a loss in HCN channel function could augment T-type Ca^{2+} channel activity. T-type Ca^{2+} channels are low threshold VGCCs that typically activate at potentials more positive to –75 mV[43, 44]. Interestingly, native as well as heterogously-expressed Ca$_V$3.1- 3.3 channels inactivate at potentials below –55 mV–60 mV[43, 44]. Hence, there is a small "window" during which these channels are active. Since T-type Ca^{2+} channel blockers had no effect on basal wildtype mEPSC frequency (Supplementary Fig 5) and the basal frequency between *Ca$_V$3.2–/–* and wildtype was similar (Supplementary Table 4), despite Ca$_V$3.2 immunogold particles being present on wildtype synaptic terminals (Fig 6b), it implies that these channels are inactive at rest. A reduction in HCN channel activity hyperpolarizes the membrane[1, 4] and thus one possibility is that RMP hyperpolarization relieves T-type Ca^{2+} channel inactivation. To investigate this hypothesis, we lowered external K$^+$ concentration from 2.5 mM to 1.75 mM, which, using the Nernst equation, is estimated to hyperpolarize the RMP by ~10 mV. Indeed, reducing external K$^+$ concentration

resulted in EC layer III neuronal hyperpolarization by 7.3 ± 0.9 mV (n=3). Further, switching from 2.5 mM to 1.75 mM K^+ significantly enhanced wildtype mEPSC frequency within 10 min by $91.6 \pm 14.1\%$ (n=6, p < 0.01, Fig 7a, c). This was restored to near control levels by adding mibefradil[41] (10 μM; Fig 7a). Interestingly, changing the external K^+ from 2.5 mM to 1.75 mM in *HCN1–/–* slices, where the RMP is expected to be approximately -80 mV[4], had little effect on mEPSC frequency (% increase = $-1.5 \pm 3.6\%$, n=5, Fig 7b), presumably as T-type Ca^{2+} channel activity was not further altered. The outward holding current, mEPSC amplitude or kinetics were not affected by reducing external K^+ concentration in wildtype or *HCN1–/–* neurons (Fig 7a, b). These results provide additional support for the notion that T-type Ca^{2+} channels are present on pre-synaptic terminals and can contribute to synaptic release under certain conditions.

HCN channels modulates evoked release onto EC layer III neurons

We also asked if HCN channels affect evoked release too. To determine this, we stimulated EC layer III distal dendrites to evoke pairs of EPSCs at 20 Hz in the absence and presence of 15 μM ZD7288 (see **Methods**). ZD7288 (15 μM) was included in the intracellular solution to block post-synaptic HCN channels. The amplitude of the first EPSC was adjusted between 50 to 100 pA (average amplitude = 71.3 ± 9.8 pA). Single EPSCs were also elicited in between pairs of EPSCs. Subtraction of these from the pairs of EPSCs was then used to elucidate the amplitudes of the first and second EPSCs within the pairs (Fig 8). Paired pulse ratio (PPR) was calculated as the amplitude of the second EPSC divided by the amplitude of the first. Under control conditions, the average PPR was 0.9 ± 0.1 (n=5, Fig 8). 15 min bath application of ZD7288 reduced PPR significantly to 0.7 ± 0.1 (n=5, p < 0.01, Fig 8) and increased the amplitude of the first evoked EPSC by $16.7 \pm 5.8\%$ (n=6, p < 0.01). In addition, square of the coefficient of variation (CV^2) decreased significantly to 0.7 ± 0.1 (p < 0.01). In contrast, ZD7288 (15 μM) had no effect on PPR in *HCN1–/–* neurons (PPR ratio before and after ZD7288 = 1.1 ± 0.2 and 1.1 ± 0.1, n=6, p = 0.92). The lowered PPR and CV^2 in wildtypes indicate that synaptic release was enhanced by pharmacological block of HCN channels. These findings, therefore, demonstrate that pre-synaptic HCN channels affect multiple modes of synaptic transmission.

Discussion

The significant findings of this study are that functional HCN1 channels are present on glutamatergic synaptic terminals synapsing onto EC layer III neurons where they reduce spontaneous and evoked neurotransmitter release. These effects are at least partly due to altered availability of low-threshold, voltage-gated T-type Ca^{2+} channel. In support, electron microscopy showed that HCN1 and $Ca_V3.2$ subunits co-exist on EC pre-synaptic terminals. As EC layer III neurons have been suggested to play significant roles in processes such as spatial navigation[22] and learning and memory[23] and HCN channel function has been associated with modification of neural network rhythms and memory formation[8], the dynamic modulation of synaptic inputs onto these neurons by HCN and T-type Ca^{2+} channels may contribute to the regulation and modulation of these physiological states.

Although HCN1 and HCN2 subunits are both expressed in the EC[3], our results suggest that HCN1 subunits are likely to predominantly contribute to the formation of pre-synaptic HCN channels in glutamatergic synapses in the EC. Indeed, HCN1 subunit immunoreactivity was detected on the active zone of wildtype excitatory synaptic terminals in the adult EC (Fig 3). Spontaneous glutamatergic synaptic transmission was also augmented in *HCN1–/–* slices and was not further affected by the non-selective HCN channel blockers, ZD7288 (Fig 1) and zatebradine (Supplementary Fig 1). These agents, on the other hand, enhanced wildtype mEPSC frequency (Fig 1, Supplementary Fig 1). Further, ZD7288 reduced the wildtype

EPSC paired pulse ratio (Fig 8). These findings indicate that pharmacological inhibition of HCN channels in normal tissue enhances glutamtergic synaptic transmission. Since ZD7288 has also been suggested to depress synaptic transmission independently of affecting HCN channels[26], it is possible that the observed effects of ZD7288 might be underestimated (Fig 1, Fig 8). Further, the effects of zatebradine are dependent upon HCN channels being open[27], [28] and therefore, the increase in mEPSC frequency in the presence of this compound may also be undervalued (Supplementary Fig 1). This might account for the increase in spontaneous release in *HCN1–/–* slices being much greater than that obtained with application of pharmacological blockers on wildtype slices (Fig 1, Supplementary Fig 1). Notwithstanding, our results provide strong support for the involvement of HCN1 channels in modulating EC excitatory synaptic transmission.

Remarkably, our results suggest that the presence of pre-synaptic HCN channels depolarizes the RMP, thereby restricting Ca^{2+} entry via pre-synaptic T-type Ca^{2+} channel activity and preventing glutamate release (**Figs** 4 –7). This suggests that pre-synaptic HCN channels may provide an additional regulatory mechanism for controlling synaptic release at these synapses. Hence, by affecting T-type Ca^{2+} channel activity, modulation of HCN channel activity by protein kinases or phosphatases will alter synaptic transmission at these synapses. Indeed, EC synaptic terminals may have functional metabotropic glutamate receptors[45], activation of which could potentially reduce HCN channel activity by altering kinase activity and induce plasticity[10].

Altered T-type Ca^{2+} channel activity by HCN channels has been suggested to occur in hippocampal dendrites too[7] and it is, therefore, tempting to speculate that this might be a universal mechanism by which these channels affect neuronal excitability. Fascinatingly, though, in invertebrate neurons, I_h has been shown to increase excitatory synaptic release in a "non-ionic" way via a pathway involving actin depolymerization[18]. It is possible that this might occur in some mammalian interneurons too[16], [17]. This therefore suggests that HCN channels in synaptic terminals may have multiple roles: a "non-ionic" purpose whereby they modulate release by processes that involve changes in the cytoskeleton and a more conventional function in which they influence synaptic transmission by modifying the terminal RMP as well as the membrane resistivity, which has been shown to occur post-synaptically in dendrites[4], [24]. Which role they adopt may depend on their location within a synapse as well as their proximity to other proteins and ion channels.

Interestingly, the expression of HCN channel subunits and their effects on synaptic release were restricted to a subset of EC glutamatergic synaptic terminals (**Figs** 1-3). This suggests that there may be factors that control expression of HCN channels in specific synapses and not others. These synapses may belong to a particular cell type. Indeed, synapses targeting EC layer III neurons can originate from a number of sources, including other EC layer III neurons, layer V and pre-subicular neurons. Since HCN subunits have not been detected in the temporoammonic (TA) pathway, EC layer III pyramid axons, or terminals synapsing onto CA1 dendrites (which belong to the TA pathway)[13], it is likely that HCN channels are present on those synaptic terminals originating from EC layer V or pre-subiculum. Further work is, therefore, required to resolve whether HCN subunit expressing synapses belong to a particular cell type and whether these synaptic terminals contain or lack proteins that regulate HCN channel expression. In addition, it remains to be determined if other cortical synapses express functional pre-synaptic HCN and T-type Ca^{2+} channels. Nonetheless, our results show that functional HCN channels can be present pre-synaptically as well as on pyramid cell dendrites in the mature cortex. Thus there may be multiple means by which HCN channels can affect neural network excitability and ultimately processes such as learning and memory.

Supplementary Material

Refer to Web version on PubMed Central for supplementary material.

Acknowledgments

Appendix

Methods

Slice preparation and electrophysiological experiments

HCN1[46] and $Ca_V3.2$[42] heterozygote breeding pairs were used to generate HCN1 null (*HCN1–/–*), $Ca_V3.2$ null (*$Ca_V3.2$–/–*) and wildtype littermates as described in Huang et al. (2009)[4]. All electrophysiological experiments involving transgenic mice were done blindly. Entorhinal-hippocampal slices were obtained from 6-9 week old *HCN1–/–, $Ca_V3.2$–/–* and wildtype mice as described previously (see [4]). For electrophysiological recordings, slices were placed in a chamber containing external solution of the following composition (mM): 125 NaCl, 2.5 KCl, 1.25 NaH_2PO_4, 25 $NaHCO_3$, 2 $CaCl_2$, 2 $MgCl_2$, 10 glucose, 0.001 tetrodotoxin; bubbled with 95% O_2/5% CO_2 (pH 7.2). Whole-cell voltage-clamp recordings were obtained from the soma and dendrites of EC neurons. The internal recording pipette solution for mEPSC recordings was composed of (in mM): 120 $KMeSO_4$, 20 KCl, 10 HEPES, 2 $MgCl_2$, 0.2 EGTA, 4 Na_2-ATP, 0.3 Tris-GTP, 14 Tris-phosphocreatine, 0.015 ZD7288; pH was adjusted to 7.3 with KOH. In some experiments, $CsMeSO_4$ was used instead of $KMeSO_4$. To record mIPSCs, $KMeSO_4$ was replaced with KCl. Pipettes containing any of these internal solutions had resistances of 5 – 12 MΩ. In some recordings, biocytin (0.4% w/v; Vector Laboratories Ltd) was included in the intracellular pipette solution. Slices were fixed in 4% paraformaldehyde and stained with streptavidin Alexa Fluor 294 conjugate (Molecular Probes Ltd) 24 hr later as described previously[47]. For paired pulse recordings, tungsten electrodes (Biomedical Instruments, Germany) placed in EC layer I approx. 50 -100 μm from EC layer III distal dendrites were used to elicit single and 20 Hz pairs of synaptic potentials in interleaved sequences every 30 s. The recordings were obtained using a Axopatch 200B amplifier (Molecular Devices, UK), filtered at 1 kHz and sampled at 10 kHz. Series resistance was usually in the order of 10-30 MΩ and was approx. 70% compensated. Recordings were discarded if the series resistance increased by more than 20% during the course of the recordings. Data were acquired using pClamp 8.2 or pClamp 10.0 (Molecular Devices, UK).

Data Analysis—mEPSC and mIPSC recordings were analysed using Mini-analysis program (v6.07, Synpatosoft, USA). Events > 1.5 pA in amplitude (i.e. all events above

baseline noise level) and with rise times of < 2 ms were detected and used for analysis. Decay times and amplitudes of these events were obtained by fitting the averaged EPSC or IPSC with a single exponential equation:

$$I(t) = A \quad \exp(-t/\pi)$$

where I is the current amplitude at any given time (t), A is the peak amplitude of the EPSC or IPSC and τ is the decay time constant.

For paired pulse experiments, data were analysed using pClamp 10.0 (Molecular Devices, UK). Interleaved single EPSCs evoked were subtracted from paired EPSCs to obtain the amplitude of the second EPSC (see Fig 8). The paired pulse ratio was then calculated as the amplitude of the second EPSC divided by the first. The square of the coefficient of variation (CV^2) was calculated as

$$\text{Coefficient Of Variation}^2 = \frac{SD_{PSC}^2 - SD_{Baseline}^2}{Mean_{Amp.}^2}$$

where SD_{PSC}^2 is the standard deviation of the EPSC amplitude squared, $SD_{Baseline}^2$ is the standard deviation of the background noise squared and $Mean_{Amp}$ is the mean amplitude of the EPSC.

Group data are expressed as mean ± SEM. Statistical significance was determined using either paired or unpaired Student's T tests as appropriate. Statistical significance of $p < 0.05$ is indicated as * in all figures.

HCN1 and $Ca_V3.2$ immunoreactivity experiments

All experiments involving transgenic mice were performed blindly. Procedures for the isolation of brain tissue from adult wildtype, *HCN1−/−* and *Ca_V3.2−/−* mice for immunohistochemistry and immunoelectron microscopy experiments before and after embedding were described previously[48]. Three antibodies were used: a monoclonal anti-HCN1 antibody was obtained from NeuroMab (USA); a polyclonal anti-HCN1 antibody was obtained from Alomone Labs (Israel); and a monoclonal $Ca_V3.2$ antibody was obtained from Neuromab. To examine the precise subcellular localization of HCN1 and $Ca_V3.2$ channels in the mouse entorhinal cortex, single and double labelling technique were used, as described previously[15].

When a single primary antibody was used, it was visualized by the silver-intensified immunogold reaction. In co-labeling experiments, HCN1 immunoreactivity was visualized by the immunoperoxidase reaction, and $Ca_V3.2$ immunoreactivity was revealed with the silver-intensified immunogold reaction. Briefly, free-floating sections were obtained from 8-9 week old mice. Sections were then incubated for 48 h with either HCN1 antibody alone or a mixture of two HCN1 and $Ca_v3.2$ antibodies, at a final protein concentration of 1-2 μg/ml each. After primary antibody incubation, the sections were incubated at 4°C overnight with secondary antibodies: biotinylated goat anti-rabbit (diluted 1:100; Vector Laboratories) and goat anti-mouse (Fab fragment, diluted 1:100) coupled to 1.4 nm gold (Nanoprobes, Stony Brook, NY) antibodies. After washes in TBS, sections were washed in double-distilled water, followed by silver enhancement of the gold particles with an HQ Silver kit (Nanoprobes, Stony Brook, NY) for 8-10 min. Subsequently for double labelling, the sections were incubated for 4 hours in the ABC complex (Vector Laboratories) made up in TBS and then washed in TB. Peroxidase was visualized with DAB (0.05% in TB, pH 7.4)

using 0.01% H_2O_2 as substrate for 5-10 min. The sections were washed in PB and then post-fixed with OsO_4 (1% in 0.1 M PB), followed by block-staining with uranyl acetate, dehydration in graded series of ethanol and flat-embedding on glass slides in Durcupan (Fluka) resin. Regions of interest were cut at 70-90 nm thick sections using an ultramicrotome (Reichert Ultracut E, Leica, Austria). Ultrathin sections were mounted on 200-mesh nickel grids. Staining was performed on drops of 1% aqueous uranyl acetate followed by Reynolds's lead citrate. Ultrastructural analyses were performed in a Jeol-1010 electron microscope. Unless otherwise stated, electron microscopic samples were obtained from three different mice and three blocks of each animal were cut for electron microscopy. Electron micrographs were captured with CCD camera (Mega View III; Soft Imaging System, Germany). Digitized electron images were then modified for brightness and contrast by using Adobe PhotoShop CS1 (Mountain View, CA) to optimize them for printing.

Quantitative analysis—To establish the relative abundance of HCN1 in EC layer III, immunolabeling quantification was performed from 60 μm coronal slices as previously described[49]. Randomly selected areas were captured at a final magnification of 45,000X, and measurements covered a total section area of ~5000 mm^2. Dendritic shafts, dendritic spines and axon terminals were assessed for the presence of immunoparticles. The percentage of immunoparticles for HCN1 at post- and presynaptic sites was calculated.

Estimation of number of synapses

6-9 week old mice were anaesthetised and perfused intracardially with a 3% glutaraldehyde in 0.05M sodium cacodylate buffer (pH 7.4). The brains were removed and incubated in 1% OsO_4 for 3 hr at 4°C. The tissue was then washed with distilled water followed by 70% ethanol, 90% ethanol and 100% ethanol. The region of interest was then embedded in a beam capsule using a neat araldite CY212 resin mixture and polymerized for 3 days at 60°C. Ultrathin sections were cut on a Reichert UCT at 85nm using a Diatome Ultra diamond knife, and collected on 400 mesh copper grids. Sections were subsequently stained was with 25% Uranyl acetate in methanol and Reynolds lead citrate and imaged using a Phillips CM 10 TEM. Electron micrographs were captured using a high sensitivity digital camera and synapses counted from digital images.

Western blot analysis

EC samples from 6-8 week old wildtype and *HCN1−/−* or *Ca$_V$3.2−/−* mice were homogenized using a syringe and sonicated for 10 s in 50 mM Tris pH 7.4, 50 mM NaCl, 2 mM EDTA, 25 mM N-ethyl maleimide, with complete protease inhibitors (Roche). The buffer was then supplemented with Igepal and SDS to final concentrations of 1 % and 0.2 %, respectively. Samples were kept on ice for 30 - 45 min and centrifuged for 30 min at 60000 x g. The pellet was discarded and the supernatant kept for SDS-PAGE analysis. The protein concentration of each sample was determined using a Bradford-based assay (Biorad). The amount corresponding to 50 μg of total protein was supplemented with gel loading buffer (50 mM Tris pH7.4, 100 mM DTT, 2 % SDS, 0.02% bromophenol blue, 2% glycerol), loaded onto a 3 – 8 % Tris – acetate gel and subjected to SDS-PAGE following the manufacturer's instructions (Invitrogen). The transfer was performed on a PVDF membrane in a semi-dry chamber (Biorad). A slice of the membrane containing proteins larger than 150 kD was incubated with anti-Ca$_V$3.2 antibody (Neuromab, dilution 1:250), regions of same membrane containing proteins of lower molecular weight was incubated with either anti-HCN1 (Neuromab, dilution 1:3000) or anti-GAPDH antibody (Sigma, dilution 1:25,000), followed by the appropriate secondary antibodies conjugated to horseradish peroxidise, and enhanced chemiluminescence detection, using a Typhoon 9410 Variable Mode Imager (APB), set in chemiluminescence mode. The protein bands were background-subtracted and the signal quantified using Imagequant v5.2. The same amount

of total protein was loaded for all samples on each gel, for accurate comparison between lanes, and the data were normalized to the corresponding GAPDH signal.

References

1. Biel M, Wahl-Schott C, Michalakis S, Zong X. Hyperpolarization-activated cation channels: from genes to function. Physiol Rev. 2009; 89:847–885. [PubMed: 19584315]

2. Lorincz A, Notomi T, Tamas G, Shigemoto R, Nusser Z. Polarized and compartment-dependent distribution of HCN1 in pyramidal cell dendrites. Nat Neurosci. 2002; 5:1185–1193. [PubMed: 12389030]

3. Notomi T, Shigemoto R. Immunohistochemical localization of Ih channel subunits, HCN1-4, in the rat brain. J. Comp Neurol. 2004; 471:241–276. [PubMed: 14991560]

4. Huang Z, Walker MC, Shah MM. Loss of dendritic HCN1 subunits enhances cortical excitability and epileptogenesis. J Neurosci. 2009; 29:10979–10988. [PubMed: 19726656]

5. Magee JC. Dendritic lh normalizes temporal summation in hippocampal CA1 neurons. Nat Neurosci. 1999; 2:508–514. [PubMed: 10448214]

6. George MS, Abbott LF, Siegelbaum SA. HCN hyperpolarization-activated cation channels inhibit EPSPs by interactions with M-type K^+ channels. Nat Neurosci. 2009; 12:577–584. [PubMed: 19363490]

7. Tsay D, Dudman JT, Siegelbaum SA. HCN1 channels constrain synaptically evoked Ca^{2+} spikes in distal dendrites of CA1 pyramidal neurons. Neuron. 2007; 56:1076–1089. [PubMed: 18093528]

8. Nolan MF, et al. A behavioral role for dendritic integration: HCN1 channels constrain spatial memory and plasticity at inputs to distal dendrites of CA1 pyramidal neurons. Cell. 2004; 119:719–732. [PubMed: 15550252]

9. Wang M, et al. Alpha2A-adrenoceptors strengthen working memory networks by inhibiting cAMP-HCN channel signaling in prefrontal cortex. Cell. 2007; 129:397–410. [PubMed: 17448997]

10. Brager DH, Johnston D. Plasticity of intrinsic excitability during long-term depression is mediated through mGluR-dependent changes in I_h in hippocampal CA1 pyramidal neurons. J Neurosci. 2007; 27:13926–13937. [PubMed: 18094230]

11. Campanac E, Daoudal G, Ankri N, Debanne D. Downregulation of dendritic I_h in CA1 pyramidal neurons after LTP. J Neurosci. 2008; 28:8635–8643. [PubMed: 18716222]

12. Fan Y, et al. Activity-dependent decrease of excitability in rat hippocampal neurons through increases in I_h. Nat Neurosci. 2005; 8:1542–1551. [PubMed: 16234810]

13. Bender RA, et al. Localization of HCN1 channels to presynaptic compartments: novel plasticity that may contribute to hippocampal maturation. J Neurosci. 2007; 27:4697–4706. [PubMed: 17460082]

14. Boyes J, Bolam JP, Shigemoto R, Stanford IM. Functional presynaptic HCN channels in the rat globus pallidus. Eur J Neurosci. 2007; 25:2081–2092. [PubMed: 17439493]

15. Lujan R, Albasanz JL, Shigemoto R, Juiz JM. Preferential localization of the hyperpolarization-activated cyclic nucleotide-gated cation channel subunit HCN1 in basket cell terminals of the rat cerebellum. Eur J Neurosci. 2005; 21:2073–2082. [PubMed: 15869503]

16. Aponte Y, Lien CC, Reisinger E, Jonas P. Hyperpolarization-activated cation channels in fast-spiking interneurons of rat hippocampus. J Physiol. 2006; 574:229–243. [PubMed: 16690716]

17. Southan AP, Morris NP, Stephens GJ, Robertson B. Hyperpolarization-activated currents in presynaptic terminals of mouse cerebellar basket cells. J Physiol. 2000; 526(Pt 1):91–97. [PubMed: 10878102]

18. Beaumont V, Zhong N, Froemke RC, Ball RW, Zucker RS. Temporal synaptic tagging by I_h activation and actin: involvement in long-term facilitation and cAMP-induced synaptic enhancement. Neuron. 2002; 33:601–613. [PubMed: 11856533]

19. Beaumont V, Zucker RS. Enhancement of synaptic transmission by cyclic AMP modulation of presynaptic Ih channels. Nat Neurosci. 2000; 3:133–141. [PubMed: 10649568]

20. Cuttle MF, Rusznak Z, Wong AY, Owens S, Forsythe ID. Modulation of a presynaptic hyperpolarization-activated cationic current (I_h) at an excitatory synaptic terminal in the rat auditory brainstem. J Physiol. 2001; 534:733–744. [PubMed: 11483704]

21. Stevens CF. Presynaptic function. Curr Opin Neurobiol. 2004; 14:341–345. [PubMed: 15194114]

22. Brun VH, et al. Impaired spatial representation in CA1 after lesion of direct input from entorhinal cortex. Neuron. 2008; 57:290–302. [PubMed: 18215625]

23. Remondes M, Schuman EM. Role for a cortical input to hippocampal area CA1 in the consolidation of a long-term memory. Nature. 2004; 431:699–703. [PubMed: 15470431]

24. Shah MM, Anderson AE, Leung V, Lin X, Johnston D. Seizure-induced plasticity of h channels in entorhinal cortical layer III pyramidal neurons. Neuron. 2004; 44:495–508. [PubMed: 15504329]

25. Williams SR, Mitchell SJ. Direct measurement of somatic voltage clamp errors in central neurons. Nat Neurosci. 2008; 11:790–798. [PubMed: 18552844]

26. Chevaleyre V, Castillo PE. Assessing the role of Ih channels in synaptic transmission and mossy fiber LTP. Proc Nat Acad Sci USA. 2002; 99:9538–9543. [PubMed: 12093909]

27. Gill CH, et al. Characterization of the human HCN1 channel and its inhibition by capsazepine. Brit J Pharmacol. 2004; 143:411–421. [PubMed: 15351778]

28. Pape HC. Specific bradycardic agents block the hyperpolarization-activated cation current in central neurons. Neuroscience. 1994; 59:363–373. [PubMed: 7516499]

29. Magee JC. Dendritic integration of excitatory synaptic input. Nat. Neurosci. Rev. 2000; 1:181–190.

30. Sun J, et al. A dual-Ca2+-sensor model for neurotransmitter release in a central synapse. Nature. 2007; 450:676–682. [PubMed: 18046404]

31. Daw MI, Tricoire L, Erdelyi F, Szabo G, McBain CJ. Asynchronous transmitter release from cholecystokinin-containing inhibitory interneurons is widespread and target-cell independent. J Neurosci. 2009; 29:11112–11122. [PubMed: 19741117]

32. Hefft S, Jonas P. Asynchronous GABA release generates long-lasting inhibition at a hippocampal interneuron-principal neuron synapse. Nat Neurosci. 2005; 8:1319–1328. [PubMed: 16158066]

33. Neher E, Sakaba T. Multiple roles of calcium ions in the regulation of neurotransmitter release. Neuron. 2008; 59:861–872. [PubMed: 18817727]

34. Groffen AJ, et al. Doc2b Is a High-Affinity Ca^{2+} Sensor for Spontaneous Neurotransmitter Release. Science (New York, N.Y). 2010; 327:1614–1618.

35. Catterall WA. Structure and function of neuronal Ca^{2+} channels and their role in neurotransmitter release. Cell Calcium. 1998; 24:307–323. [PubMed: 10091001]

36. Tsien RW, Ellinor PT, Horne WA. Molecular diversity of voltage-dependent Ca2+ channels. Trends Pharmacol Sci. 1991; 12:349–354. [PubMed: 1659003]

37. Bourinet E, et al. Interaction of SNX482 with domains III and IV inhibits activation gating of alpha(1E) (Ca(V)2.3) calcium channels. Biophys J. 2001; 81:79–88. [PubMed: 11423396]

38. Dreyfus FM, et al. Selective T-type calcium channel block in thalamic neurons reveals channel redundancy and physiological impact of I_T window. J Neurosci. 2010; 30:99–109. [PubMed: 20053892]

39. Shipe WD, et al. Design, synthesis, and evaluation of a novel 4-aminomethyl-4-fluoropiperidine as a T-type Ca^{2+} channel antagonist. J Med Chem. 2008; 51:3692–3695. [PubMed: 18540666]

40. Uebele VN, et al. T-type calcium channels regulate cortical plasticity in-vivo. [corrected]. Neuroreport. 2009; 20:257–262. [PubMed: 19212242]

41. Randall AD, Tsien RW. Contrasting biophysical and pharmacological properties of T-type and R-type calcium channels. Neuropharmacology. 1997; 36:879–893. [PubMed: 9257934]

42. Chen CC, et al. Abnormal coronary function in mice deficient in alpha1H T-type Ca2+ channels. Science (New York, N.Y). 2003; 302:1416–1418.

43. Crunelli V, Toth TI, Cope DW, Blethyn K, Hughes SW. The 'window' T-type calcium current in brain dynamics of different behavioural states. J. Physiol. 2005; 562:121–129. [PubMed: 15498803]

44. Talavera K, Nilius B. Biophysics and structure-function relationship of T-type Ca^{2+} channels. Cell Calcium. 2006; 40:97–114. [PubMed: 16777221]

45. Evans DI, Jones RS, Woodhall G. Activation of presynaptic group III metabotropic receptors enhances glutamate release in rat entorhinal cortex. J Neurophysiol. 2000; 83:2519–2525. [PubMed: 10805653]

46. Nolan MF, et al. The hyperpolarization-activated HCN1 channel is important for motor learning and neuronal integration by cerebellar Purkinje cells. Cell. 2003; 115:551–564. [PubMed: 14651847]

47. Cossart R, et al. Dendritic but not somatic GABAergic inhibition is decreased in experimental epilepsy. Nat Neurosci. 2001; 4:52–62. [PubMed: 11135645]

48. Lujan R, Shigemoto R. Localization of metabotropic GABA receptor subunits GABAB1 and GABAB2 relative to synaptic sites in the rat developing cerebellum. Eur J Neurosci. 2006; 23:1479–1490. [PubMed: 16553611]

49. Lujan R, Nusser Z, Roberts JD, Shigemoto R, Somogyi P. Perisynaptic location of metabotropic glutamate receptors mGluR1 and mGluR5 on dendrites and dendritic spines in the rat hippocampus. Eur J Neurosci. 1996; 8:1488–1500. [PubMed: 8758956]
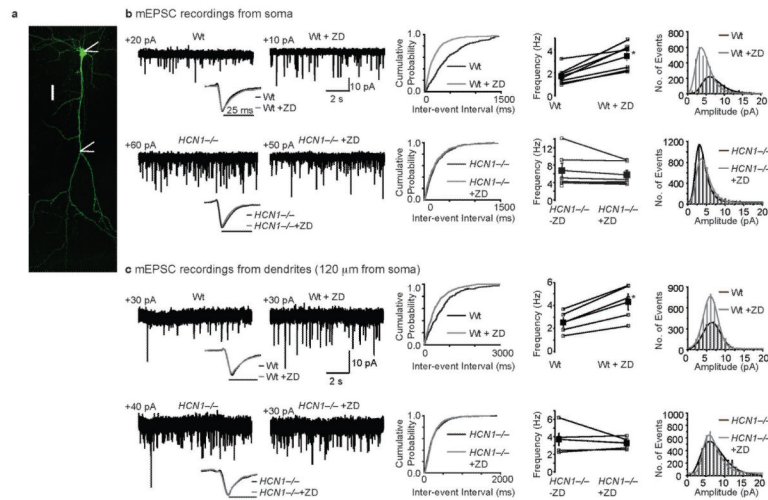
Figure 1. Pharmacological block or deletion of HCN channels enhances mEPSC frequency in EC layer III pyramids

a Morphology of typical mouse EC layer III pyramidal neuron. The scale represents 20 μm. **b** and **c** Example mEPSC recordings from wildtype (Wt) and *HCN1−/−* soma and dendrites before and after 15 min bath application of the HCN channel blocker, ZD7288 (ZD; 15 μM). The cumulative probability curves for each recording are displayed above the trace and on the right respectively. The average normalized mEPSCs obtained from the recordings are also presented. The scale shown in the upper panel of **b** and **c** applies to all traces within those panels. Graphs depicting the mean (filled squares) and standard error of Wt and *HCN1−/−* soma and dendritic mEPSC frequency in the absence and presence of ZD7288 are also shown. Open squares illustrate the mEPSC frequency from individual experiments. On the far left of each panel are the amplitude histograms for the total number of mEPSCs obtained from Wt soma (n=7), Wt dendrites (n=5), *HCN1−/−* soma (n=6) and *HCN1−/−* dendrites (n=5) with and without ZD7288. Superimposed on the histograms are Gaussian fits to demonstrate the peak amplitude of mEPSCs.
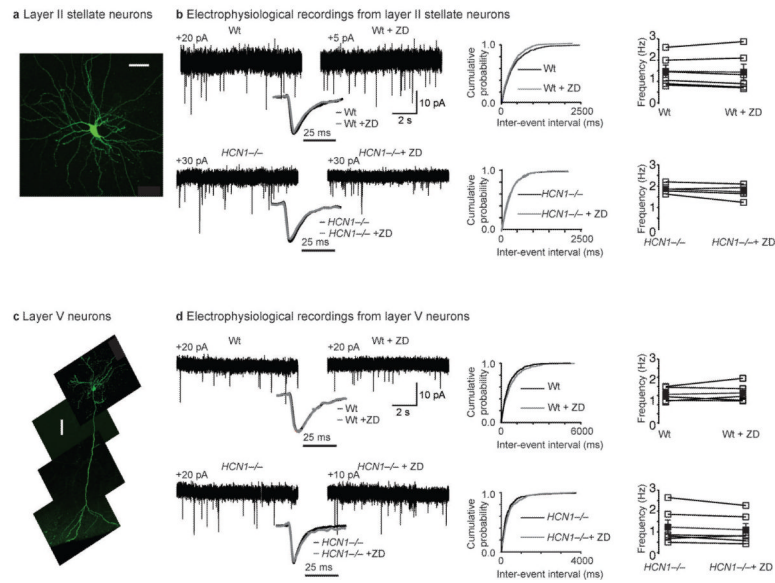
**Figure 2. HCN channel block or deletion has no effect on mEPSCs onto EC layer II and layer V neurons**
a and **c** Typical morphologies of mouse EC layer II stellate cell and layer V neuron. The scale bar in **a** and **b** represent 20 μm and 50 μm respectively. **b** and **d** Representative mEPSC recordings from wildtype (Wt) and *HCN–/–*layer II stellate and layer V pyramid soma before and after application of ZD7288 (ZD; 15 μM). The values above the traces indicate that outward holding current at −70 mV. The average mEPSC obtained from the recordings are displayed below the traces. The cumulative probability curves for each of the traces are also illustrated on the right of the recordings. The scale shown in the upper trace for **b** and **d** applies to all traces within **b** and **d** respectively. Graphs depicting the individual (open squares) and average (closed squares) mEPSC frequencies recorded from wildtype and *HCN–/–* stellate and layer V pyramid neurons before and after application of ZD7288 are shown at the far right in each panel.
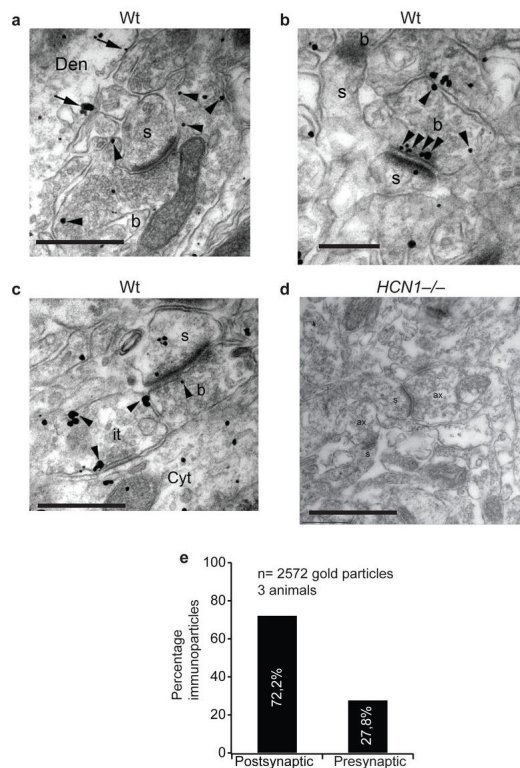
Figure 3. HCN1 subunits are localized to active zones of synaptic terminals
a, **b** Immunoparticles for HCN1 along the extrasynaptic plasma membrane (e.g. arrows) of dendritic spines (s) and shafts (Den) establishing synapses with excitatory terminals (b) in EC layer III. Pre-synaptic HCN1 subunits in excitatory terminals were mainly located in the active zone (b). **c** Although at lower proportion, immunoparticles for HCN1 were also observed in putative inhibitory axon terminals (it) (e.g. arrowheads), recognised by the shape of synaptic vesicles and the lack of a prominent postsynaptic density in the postsynaptic element, establishing synaptic contact with somata. **d** Immunoreactivity for HCN1 in EC layer III of HCN1 null mice as revealed at the electron microscopy level. No labelling could be detected in the null mice. ax, axon terminal; s, dendritic spine. **e** Quantitative analysis on the percentage of immunoparticles (n=2572) for HCN1 at post- and pre-synaptic sites in EC layer III, showed that 72% were localised at postsynaptic sites and 28% at presynaptic sites. Cyt, cytoplasm; N, nucleus. Scale bars: **a**, **c** and **d**, 0.5 μm; **b**, 0.2 μm.
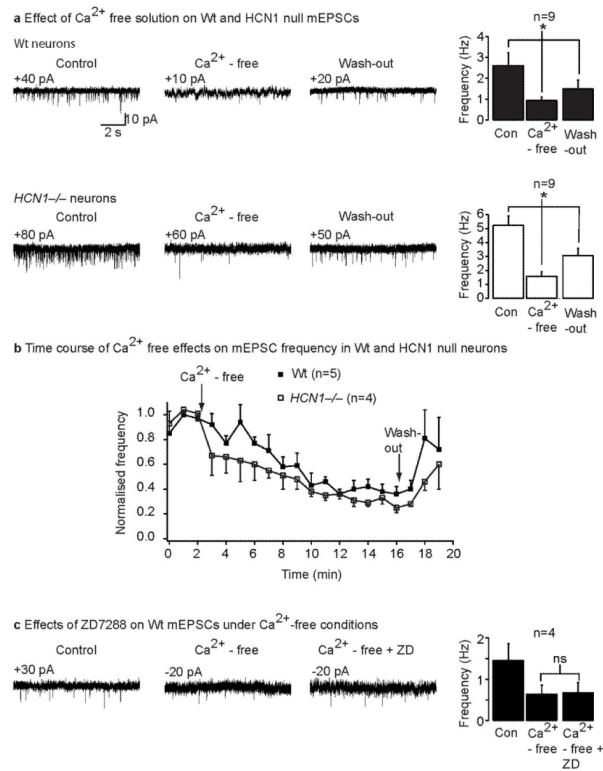
Figure 4. Ca^{2+} dependence of EC layer III mEPSCs

a Traces from wildtype (Wt) and HCN1 null neurons respectively in the absence, presence and washout of Ca^{2+} - free external solution. The outward holding current values are displayed above the traces. The mean and standard error of 9 individual experiments are shown in the bar graphs on the right. **b** Time course of the effects of applying Ca^{2+} free solution. The average frequency per minute during 5 Wt and 4 *HCN–/–* recordings was calculated and normalised. **c** Example recordings from Wt neurons under control conditions, following application of Ca^{2+}-free solution and Ca^{2+}-free solution containing ZD7288. The outward holding current values at −70 mV are indicated above the traces. The graph on the right depicts the average frequency from 4 experiments. The scale bar shown in (a) applies to all traces within the figure. Significance (p < 0.05) is indicated by an asterisk.
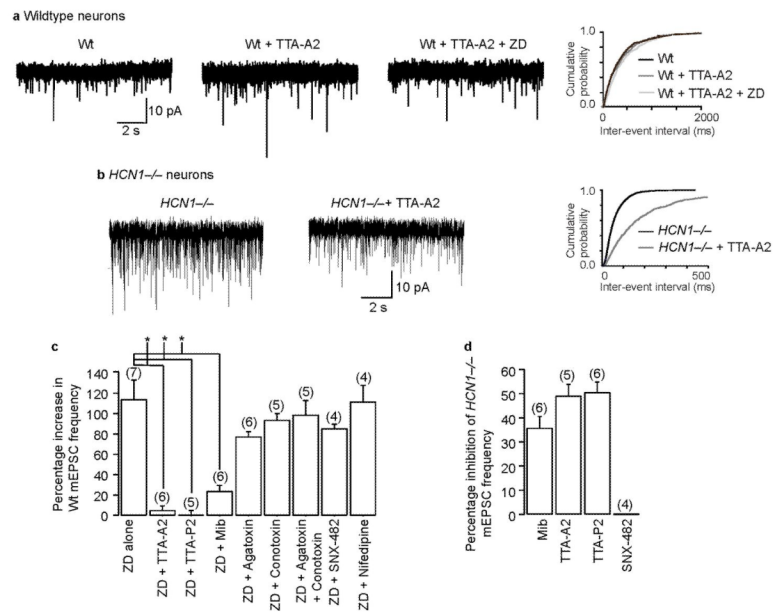
Figure 5. T-type Ca^{2+} channel blockers reduce the increase in mEPSC frequency caused by pharmacological block of I$_h$ or deletion of HCN1 subunits

a and **b** Recordings obtained in wildtype (Wt) and *HCN–/–* neurons in the absence and presence of the potent and selective T-type Ca^{2+} channel blocker, TTA-A2 (500 nM). In Wt neurons, ZD7288 was additionally applied after TTA-A2 neurons too. The outward holding current at a holding potential of –70 mV are indicated above the traces. The cumulative probability curves for all the recordings are displayed on the right in each panel. The scale bar shown in **a** and **b** applies to all traces within **a** and **b** respectively. **c** Bar graph to demonstrate the effects of co-application of ZD7288 (15 µM) and Ca^{2+} channel blockers for T- (TTA-A2 (500 nM), TTA-P2 (1 µM) and mibefradil (10 µM; Mib)), P/Q – (ω-agatoxin IVA (100 nM)), N- (ω -conotoxin GVIA (100 nM)), L- (nifedipine (2 mM)) and R- (SNX-482 (200 nM)) type Ca^{2+} channels. The effects of treatment with ZD7288 alone are also shown. **d** Graph to illustrate the effects of the T-type (TTA-A2, TTA-P2 and mibefradil (Mib)) and R-type (SNX-482) Ca^{2+} channel blockers on mEPSC frequency in HCN1 null EC layer III neurons. In **c** and **d**, the numbers of observations for each treatment are indicated above the individual bars. Asterisks indicate significance at p < 0.05.

a Immunogold labelling of Ca$_V$3.2 in wildtype and Ca$_V$3.2 null entorhinal cortex
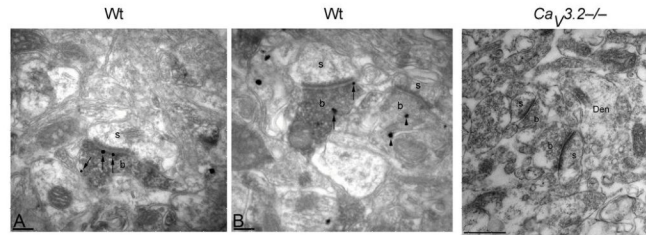
b Effects of HCN channel block on Ca$_V$3.2 wildtype and null mEPSCs.
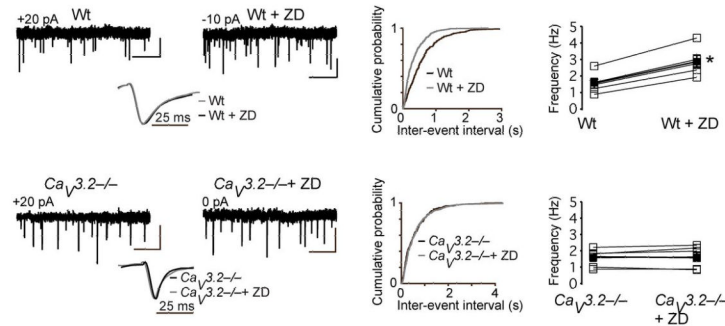
Figure 6. Ca$_V$3.2 co-localise with HCN1 at EC synaptic terminals and cause the increase in excitatory synaptic transmission following HCN1 channel inhibition

a Two typical electron micrographs showing immunoreactivity for HCN1 (peroxidase reaction product) and Ca$_V$3.2 (immuoparticles) in wildtype (Wt) sections as detected using pre-embedding double-labelling methods at EM level. Immunogold particles for Ca$_V$3.2 were absent in Ca$_V$3.2 null (*Ca$_V$3.2–/–*) sections. Axon terminals and dendritic spines are indicated by b and s respectively. Scale bars: 0.2 µm. **b** Example recordings showing the effects of 15 min bath application of ZD7288 (ZD, 15 µM) on mEPSCs recorded from Ca$_V$3.2 null (*Ca$_V$3.2–/–*) EC layer III neurons and Wt neurons. The vertical and horizontal scale bars on the traces represent 10 pA and 2 s respectively. In values above the recordings indicate the outward holding currents at −70 mV. The cumulative probability curves are shown on the right. The average normalised mEPSC traces obtained from the traces before and after ZD7288 application are shown below the recordings. The graphs on the far right depict the individual (open squares) and mean (filled squares) frequency of mEPSCs obtained from Ca$_V$3.2 Wt (n=5) and null (n=6) in the absence and presence of ZD7288. Significance at p < 0.05 is indicated by an asterisk.
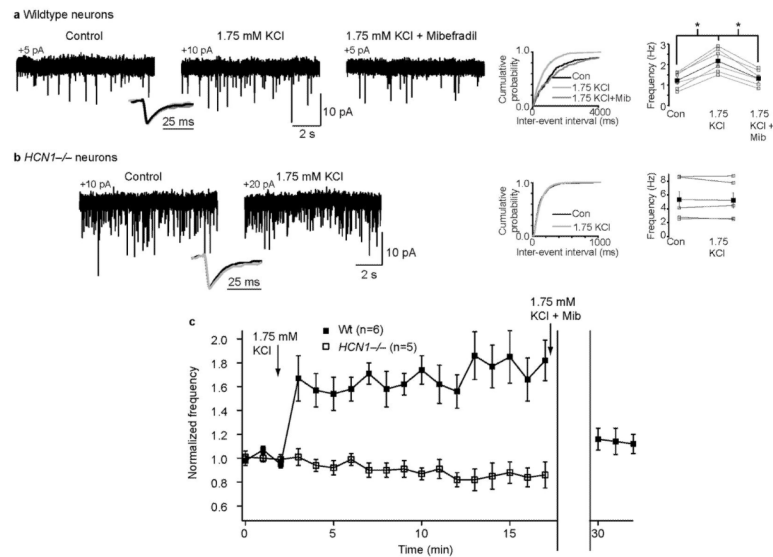
Figure 7. Hyperpolarization enhances mEPSC frequency by activating T-type Ca^{2+} channels

a and **b** Representative traces and their cumulative probability curves illustrating the effects of lowering the external K$^+$ concentration from 2.5 mM to 1.75 mM in wildtype (Wt) and HCN1 null neurons. The additional effects of mibefradil (Mib; 10 µM) on Wt mEPSCs in 1.75 mM K$^+$ are also presented. The outward holding currents at −70 mV are shown above the traces. An overlay of the average normalised EPSCs from Wt and *HCN1−/−* neurons under control conditions (black), with 1.75 mM K$^+$ (light grey) and in the presence of 1.75 mM K$^+$ and mibefradil (dark grey) are also displayed. The average mEPSC frequency (filled squares) as well as the individual frequency values obtained from each experiment (open squares) under these conditions in Wt and HCN1 null neurons are shown on the far right in each panel. The scale bar shown in **a** and **b** applies to all traces within **a** and **b** respectively. Asterisks represent significance at p < 0.05. **c** Graph showing the time course of the effects of reducing the K$^+$ concentration from 2.5 mM to 1.75 mM in Wt and *HCN1−/−* neurons. The average mEPSC frequency for each minute of the recording before and after 15 min bath application of 1.75 mM KCl is shown.
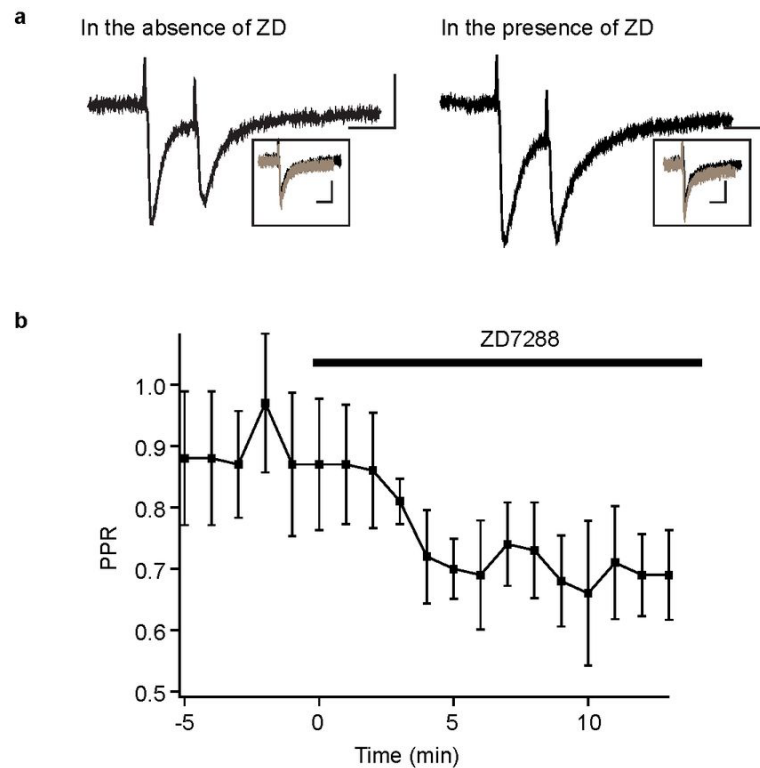
Figure 8. Effects of pharmacologically blocking HCN channels on evoked synaptic release
a Representative traces in the absence and presence of ZD7288 (ZD, 15 µM) obtained at the soma are shown above the graph. In between each paired pulse, a single stimulus was used to elicit an EPSC. By subtracting this EPSC from the paired EPSCs, the amplitude and shape of the individual EPSCs were obtained. The insets show the overlayed black (second EPSC) and grey (first EPSC) subtracted traces before and after application of ZD7288. The vertical and horizontal scale bars for the paired pulse traces as well as the subtracted traces represent 40 pA and 50 ms respectively. **b** Graph showing the effects of bath applying ZD7288 on the paired pulse ratio (PPR) in EC layer III neurons. Pairs of EPSCs were obtained every minute by stimulating the distal dendrites of EC layer III neurons.